Nature of coupling and origin of coercivity in giant magnetoresistance NiO-Co-Cu-based spin valves

Harsh Deep Chopra* and David X. Yang
Thin Films & Nanosynthesis Laboratory, Materials Program, Mechanical and Aerospace Engineering Department, State University of New York at Buffalo, Buffalo, New York 14260

P. J. Chen, D. C. Parks, and W. F. Egelhoff, Jr.
National Institute of Standards and Technology, Gaithersburg, Maryland 20899
(Received 15 July 1999)

The effect of various couplings on the switching field and coercivity in NiO-Co-Cu-based giant magnetoresistance (GMR) bottom spin valves is investigated. Bottom spin valves as well as different layer permutations that make up a bottom spin valve, viz., Co single films, Co/Cu/Co trilayers, and Co/NiO bilayers (deposited under similar growth conditions), were investigated for their magnetic, crystal, and interfacial structure. As-deposited bottom spin valves exhibit a large GMR of ≈16.5%, and a small net ferromagnetic coupling (+0.36 mT) between the ''free'' Co layer and the NiO-pinned Co layer. The high resolution transmission electron microscopy (HRTEM) and *in situ* scanning tunneling microscopy (STM) studies on spin valves and trilayers show that the average grain size in these films is ≈20 nm and average roughness ≈ 0.3 nm. Using these values, the observed ferromagnetic coupling in spin valves could largely be accounted for by Néel's so-called ''orange-peel'' coupling. Results also show that the ''free'' Co layer exhibits an enhanced coercivity ($H_c^{\text{Free-Co}} = 6.7$ mT) with respect to Co single films of comparable thickness ($H_c^{\text{Co}} = 2.7$ mT). The TEM studies did not reveal the presence of any pin-holes, and ''orange-peel'' or oscillatory exchange coupling mechanisms cannot adequately account for this observed coercivity enhancement in the ''free'' Co layer of spin valves. The present study shows that the often observed and undesirable coercivity enhancement in the ''free'' Co layer results from magnetostatic coupling between domain walls in the ''free'' Co layer and high coercivity NiO-pinned Co layer ($H_c^{\text{Pinned-Co}} \approx 45$ mT); without NiO, the coercivity of Co layers in the corresponding Co/Cu/Co trilayer remains largely unchanged ($H_c^{\text{Co/Cu/Co}} = 3.0$ mT) with respect to Co single films. Evidence of magnetostatically coupled domain walls was confirmed by direct observation of magnetization reversal, which revealed that domain walls in the ''free'' Co layer are magnetostatically locked-in with stray fields due to domain walls or magnetization ripples in the high coercivity NiO-pinned Co layer of the spin valves. The observed escape fields (defined as fields in excess of intrinsic coercivity of Co single film that are required to overcome magnetostatic coupling between domain walls) are in agreement with theoretically calculated values of escape fields.

I. INTRODUCTION

The study of magnetic properties of materials composed of alternating magnetic and nonmagnetic layers has recently attracted great attention.[1–7] In these systems, the interplay between electron transport properties and magnetic behavior results in a variety of fascinating phenomena.[8,9] In particular, recent attention has focused on the giant magnetoresistance (GMR) effect.[10,11] Several interesting phenomena, such as the oscillatory nature of exchange coupling and saturation magnetoresistance, as a function of nonmagnetic spacer layer thickness, are found to be associated with magnetic multilayers exhibiting GMR.[12] A clear understanding of underlying principles governing the manifestation of the GMR effect is important in order to understand the spin-dependent electron transport properties. It is also essential for exploiting various technological applications such as magnetic-field sensors and read heads for high-density data-storage devices.[13]

The GMR effect was originally reported in artificially layered superlattices comprised of a large number of magnetic/nonmagnetic bilayers.[10] The GMR effect in a superlattice configuration relies on antiferromagnetic coupling between adjacent magnetic layers mediated by intervening nonmagnetic spacers. Although a GMR effect as large as 80% has been reported in superlattices based on the Co-Cu system (which is the subject of the present study),[14] the switching fields required to overcome antiferromagnetic coupling in superlattice structures are large. From an application standpoint, a combination of high GMR and low switching field is required. To achieve this combination, multilayers in spin valve configurations have been proposed, viz., top,[15] bottom,[16–19] and symmetric spin valves.[16–19] The description of a spin valve as top, bottom, or symmetric refers to the position of the pinned ferromagnetic layer(s) (two in the case of symmetric spin valves, one at the top and another at the bottom). Specifically, in NiO-Co-Cu-based bottom spin valves investigated in the present study, the bottom Co layer is pinned by an adjacent antiferromagnetic layer of NiO through direct exchange anisotropy such that its magnetization vector remains unchanged in the range of applied field values necessary to switch the free Co layer. With respect to the pinned Co layer, the ''free'' Co layer flips its magnetization parallel or antiparallel in an applied field, giving rise to the GMR effect.

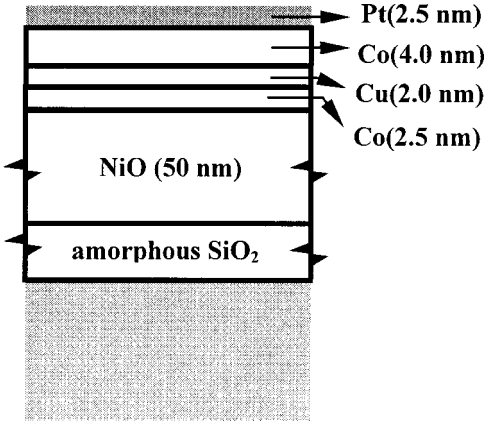

FIG. 1. Configuration of NiO-Co-Cu-based bottom spin valves investigated in the present study.

In principle, low switching fields in the ''free'' Co layer can be achieved by minimizing contributions to it from coupling with the pinned Co layer, coercivity, and anisotropy. However, a consequence of a multilayer configuration (as opposed to magnetic single films) is the existence of various interlayer magnetic interactions.[12,20–33] An ability to achieve arbitrarily low switching fields in the ''free'' Co layer of a spin valve relies on the degree of control that can be exercised during film deposition in order to eliminate or balance the magnitude of various positive and negative magnetic interactions between the layers (see Refs. 34–41, and references within). However, a difficulty in controlling contributions from various coupling mechanisms results, in large part, from an inability to make a clear distinction between them. Clearly, from a device viewpoint, it is important to identify and control the relative magnitude of each interaction, and its effect on the switching characteristics of the device. In the present study, bottom spin valves and different layer permutations that make up a bottom spin valve, namely, a Co single film, Co/Cu/Co trilayer, and Co/NiO bilayer, were deposited under similar growth conditions. These films were systematically investigated for their magnetic, crystal, and interfacial structure in order to analyze and quantitatively estimate the magnitude of the coupling strength due to different mechanisms, their manifestation during switching, and the origin of the often observed coercivity enhancement in the free Co layer of bottom spin valves. The nature of exchange anisotropy, coercivity, and details of magnetization reversal in Co/NiO direct exchange coupled bilayers are being reported elsewhere.[42] Also note that the sample size was kept sufficiently large (≈ 1 cm^2 squares) in order to minimize demagnetizing effects within various magnetic layers of the multilayers. This allows the magnitude of remaining operative coupling mechanisms to be determined in as-deposited films. Of course, in devices where the dimensions are of the order of micron or submicron, demagnetizing or stray field coupling is expected to play a significant role.

II. EXPERIMENTAL DETAILS

The NiO-Co-Cu-based bottom spin valves investigated in the present study were deposited on oxidized Si⟨100⟩ substrates, and had the following configuration: Co (4.0 nm)/Cu (2.0 nm)/Co (2.5 nm)/NiO (50 nm), as shown schematically in Fig. 1; a protective Pt or Ta film ≈ 2.5 nm thick was deposited in order to prevent oxidation of the top Co layer. In addition, several permutations that make up a bottom spin valve, viz., Co (x nm, $x = 2.5–10$ nm) single films, Co (4.0 nm)/Cu (2.0 nm)/Co (2.5 nm) trilayers, and Co (x nm; $x = 2.5–10$ nm)/NiO (50 nm) exchange anisotropy coupled bilayers, were also deposited under similar growth conditions on oxidized Si⟨100⟩ substrates. Elaborate steps were taken to remove any contamination on the substrates prior to film deposition. The cleaved substrates (≈ 1 cm^2 squares) were cleaned ultrasonically in a glassware-cleansing solution, rinsed in distilled water, and blow-dried. Care was taken to remove a hydrocarbon layer ≈ 1 nm thick that condense on the surface from ambient air, by sputtering with a neutralized beam of 100 eV argon ions. X-ray photoelectron spectroscopy confirmed the removal of the hydrocarbon layer. The films were deposited at a rate of ≈ 0.1 nm s^{-1} in 2 mTorr (≈ 0.26 Pa) Ar partial pressure in the presence of 20 mT magnetic field applied parallel to the plane of the substrates. This field produces an easy axis in Co layers, and defines the direction of exchange anisotropy in the pinned Co layer along the applied field direction. The base pressure before deposition was typically 1×10^{-8} Torr ($\approx 10^{-6}$ Pa), of which 95% was H_2 and the remainder was largely H_2O. The low base pressure was achieved, in part, by depositing a Ti film (≈ 1.5 nm) on the inside of the deposition chamber from a centrally mounted Ti filament just prior to the deposition of the metal layers.

The magnetoresistance measurements were made *in situ* using the four-point probe dc mode method. The multiplicative conversion factor from four-point resistance to sheet resistance is of the order of four, but depends on the actual dimensions of the sample. The coercivity values of Co single films and trilayers were measured from in-plane magnetization (M-H) loops obtained from a superconducting quantum interference device (SQUID) magnetometer. The coercivity value of the pinned and the ''free'' Co layers of spin valves were calculated from the high-field and low-field GMR loops. The nature of magnetization reversal was studied in real time using the high resolution interference-contrast-colloid (ICC) technique,[43] the details of which have recently been reviewed elsewhere.[44] The ICC method employs a colloidal solution to decorate the microfield on a magnetic surface, similar to the versatile Bitter technique. However, the technique differs in the manner in which the colloid-decorated microfield is detected. The ICC method uses a Nomarski interferometer to detect surface microfield distribution.[45] The magnetic microfield on a magnetic surface causes local variation in the density of colloid particles (average colloid particles size is ≈ 7 nm), thereby delineating the domain structure. This microfield is detected by polarization interferometer optics, which detects any unevenness at the nanometer level due to minute surface roughness produced by the local variation in colloid density at positions where stray fields are present, and reveals domain structure with a pronounced three-dimensional effect.[46]

The structure investigations were performed on JEOL-3010 and JEOL-2010 high-resolution transmission electron microscopes (HRTEM) operating at 300 and 200 KeV, respectively. A Gatan Image Filter on JEOL-3010 was used to directly acquire digital images, with typical magnifications

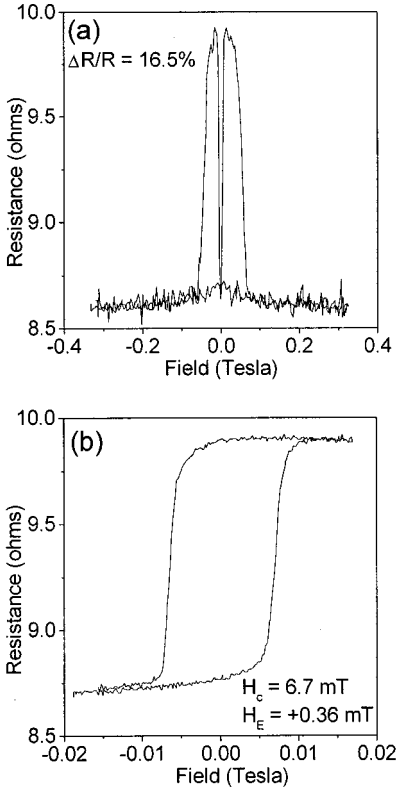

FIG. 2. (a) High-field and (b) low-field GMR loops of a typical bottom spin valve investigated in the present study.

of one million. Images were recorded at zero-loss spectrum of the electrons, which serves to enhance the overall image contrast. Observations were made on cross-sectioned samples prepared by ion-milling in a cold stage using Ar^+ ions (3.5 KeV and 1 mA). The cross-section profiles were viewed along the reference Si ⟨110⟩ zone axis.

A scanning tunneling microscope (STM) is located in a separate chamber so samples from the deposition chamber can be transferred through a vacuum interlock and characterized in vacuum. All images were recorded with a tunneling current of 2 nA, with the tip biased at +200 mV with respect to the sample. The tips were prepared from 0.25 mm diameter $Pt_{90}Ir_{10}$ wires clipped under tension with a wire cutter. Multiple images were taken at a variety of locations on each sample to ensure that the results were typical. Most STM images were recorded with a single tip, and great effort was devoted to repeat intercomparison among the samples to ensure that changing tip conditions did not change the average topographic roughness.

III. RESULTS

Figures 2(a) and 2(b) show, respectively, the high-field and low-field GMR loops of a typical bottom spin valve investigated in the present study. As seen from the high-field GMR loop in Fig. 2(a), as-deposited spin valve samples exhibit a high GMR of ≈16.5% (the highest GMR value heretofore reported in bottom spin valves being 19% by Egelhoff *et al.*[39]). In addition, the low-field GMR loop in Fig. 2(b) shows a positive shift away from the center (+0.36 mT), indicating a small net ferromagnetic coupling between the free Co layer and the NiO-pinned Co layer. The high-field

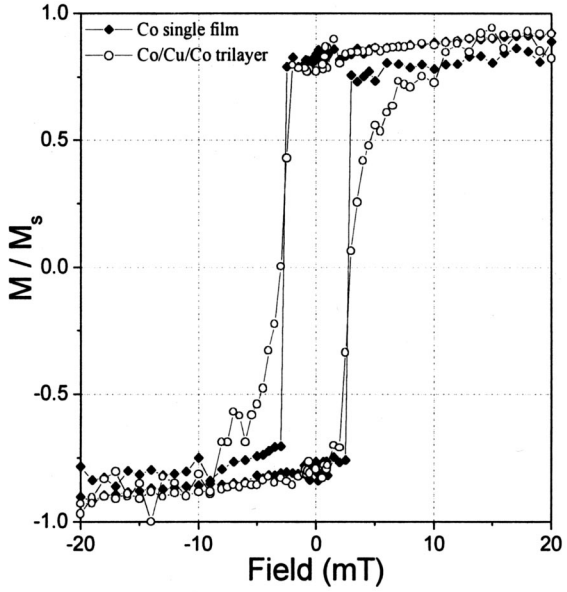

FIG. 3. Room-temperature normalized easy axis M-H curves of a Co (2.5 nm) single film and a Co (4.0 nm)/Cu (2.0 nm)/Co (2.5 nm) trilayer measured with a SQUID. Both films were deposited on oxidized Si (100) substrates.

and low-field GMR loops in Figs. 2(a) and 2(b) also provide values of coercivity of the pinned and ''free'' Co layers of spin valves, respectively. From Fig. 2(b), whereas the coercivity of the ''free'' Co layer is 6.7 mT, the bottom Co layer is strongly pinned by the antiferromagnet NiO and has a large coercivity ($H_c^{\mathrm{Pinned-Co}} \approx 45$ mT), Fig. 2(a), which is approximately seven times the coercivity of the ''free'' Co layer.

Figure 3 shows the easy axis normalized M-H curves obtained from a Co (2.5 nm) single film and a Co (4.0 nm)/Cu (2.0 nm)/Co (2.5 nm) trilayer. In addition to the largely square M-H loops for these two films, Fig. 3 shows that the coercivity of Co single film ($H_c^{\mathrm{Co}} = 2.7$ mT) is approximately 17 times lower than the coercivity of NiO-pinned Co layer in Fig. 2(a) ($H_c^{\mathrm{pinned-Co}} \approx 45$ mT), and is roughly one-third of the coercivity of the ''free'' Co layer of the bottom spin valve [$H_c^{\mathrm{Free-Co}} = 6.7$ mT as shown in Fig. 2(b)], see also Ref. 47. It is well known that in addition to exchange anisotropy, NiO is also able to induce a large coercivity in the pinned Co layer. Interestingly, however, Fig. 2(b) and Fig. 3 show that the ''free'' Co layer of spin valves also exhibits an enhanced coercivity with respect to Co single film. This enhanced coercivity could be attributed to coupling with the modified magnetization state of the NiO-pinned Co layer, because the M-H curve of the Co/Cu/Co trilayer in Fig. 3 clearly shows that in the absence of NiO, the coercivity of Co layers in the trilayer remains largely unchanged ($H_c^{\mathrm{Co/Cu/Co}} = 3.0$ mT) with respect to Co single film.

The origin of above described coercivity enhancement in the ''free'' Co layer and the nature of coupling between the ''free'' and pinned Co layers of spin valves was further investigated by studying the microscopic details of magnetization reversal. Since the existence of interlayer interactions alter the geometry of domain structure in a multilayer, magnetization reversal in a reference Co single film is described

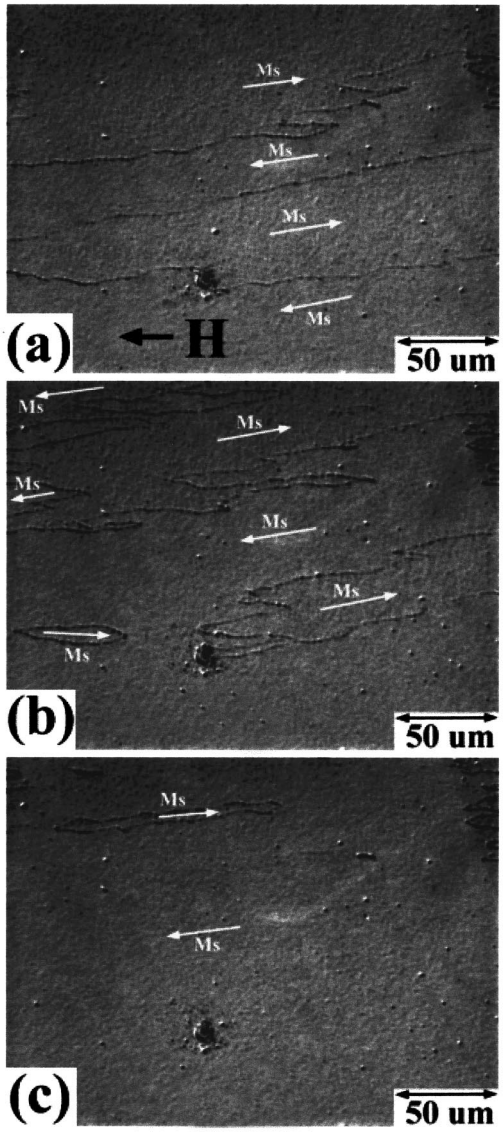

FIG. 4. ICC domain structure during magnetization reversal in a Co (2.5 nm) single film. The images were recorded using the ICC technique (see text). The direction of applied field points along the black arrow marked in Fig. 4(a), which coincides with the uniaxial anisotropy axis. The applied field values are (a) $H=2.6$ mT, (b) $H=2.7$ mT, and (c) $H=2.8$ mT. See text for explanation.

first in order to subsequently highlight the modified domain structure in the ''free'' Co layer of spin valves. Figure 4(a)–4(c) show the details of easy-axis magnetization reversal in a Co (2.5 nm) single film as a function of applied magnetic field, and whose M-H curve is shown in Fig. 3. In Figs. 4(a)–4(c), the easy axis of the film lies approximately in the horizontal direction, and the direction of applied field points from right to left. Following saturation in the positive direction, an increase in field strength in the negative direction results in nucleation of reversed domains, as shown in Fig. 4(a). The saturation magnetization vector $\mathbf{M_s}$ within these reversed domains is favorably oriented with respect to the applied field, pointing from right to left, as shown in Figs. 4(a)–4(c). Néel walls separate these reversed domains from the unfavorably oriented unreversed domains in which the $\mathbf{M_s}$ vector points from left to right, as shows in Figs. 4(a)–4(c). As the field strength was increased, reversed domains grow by consuming unfavorably oriented domains by displacement of Néel walls parallel to themselves, as shown sequentially in Figs. 4(a)–4(c). Reversal by wall motion continues with increasing field strength until the whole film becomes a single domain whose $\mathbf{M_s}$ vector points along the negative field direction. This is the expected reversal behavior of a thin uniaxial ferromagnetic single film.

Next, consider the magnetization reversal in another multilayer constituent comprising a bottom spin valve, namely, a Co(4.0 nm)/Cu (2.0 nm)/Co (2.5 nm) trilayer. The largely square M-H loop of the Co/Cu/Co trilayer in Fig. 3 indicates that, for the given nominal Cu thickness of 2.0 nm, the two Co layers are ferromagnetically coupled. Figures 5(a)–5(d) show the microscopic details of easy-axis magnetization reversal in the Co/Cu/Co trilayer. Figure 5(a) also indicates the direction of applied field in these micrographs, which coincides with the easy axis of the trilayer. Following saturation in the positive direction, Fig. 5(a) shows that remagnetization in the negative direction occurs by nucleation and growth of reversed domains. Simultaneously with the growth of these reversed domains, new reversed domains continue to nucleate locally in the film [encircled in Figs. 5(a) and 5(b)]. Within each reversed domain, the $\mathbf{M_s}$ vector is favorably oriented with respect to the applied field, as shown in Fig. 5(a). However, unlike reversed domains in the Co single film in Figs. 4, the reversed domains in the Co/Cu/Co trilayer are actually superimposed regions of the two Co layers of the trilayer, which have simultaneously undergone reversal due to positive coupling between them, as shown schematically in the cross-sectional view of the trilayer in Fig. 6. These superimposed reversed domains are separated from the unreversed regions of the film by superimposed Néel walls whose chilarity is opposite to each other. Superimposed Néel walls of opposite chilarity are energetically favorable entities due to a more complete closure of stray fields associated with them,[26–30] as shown schematically in Fig. 6. As the field strength was increased in the negative direction, reversal occurs by the collective motion of such superimposed Néel walls across the sample whereby, unfavorably oriented domains with respect to the applied field direction are consumed by the favorably oriented domains, as shown in Figs. 5(a)–5(c). As the reversed domains grow by wall motion, they leave behind several 360° walls in the trilayer, as illustrated sequentially by black arrows in Figs. 5(b)–5(d). Applied field values as high as 10–12 mT were required to completely annihilate these 360° walls; some 360° walls required even higher fields to annihilate. Note that these 360° walls are Néel walls in ferromagnetically coupled multilayers, which are trapped at inhomogeneities in the film, and their stability depends on the local variation in coupling strength.[48] It has previously been shown that their stability or pinning strength increases with a decrease in nonmagnetic spacer layer thickness,[49] being also dependent on the topography of the interfaces, as is further discussed in the following section.

Figures 7(a)–7(f) show the magnetization reversal in the ''free'' Co layer of the bottom spin valve, whose GMR loop is shown in Fig. 2(b). Note that a lower coercivity in the ''free'' Co layer ($H_c^{\text{Free-Co}}=6.7$ mT) with respect to the pinned Co layer ($H_c^{\text{Pinned-Co}}\approx 45$ mT) allows observation of

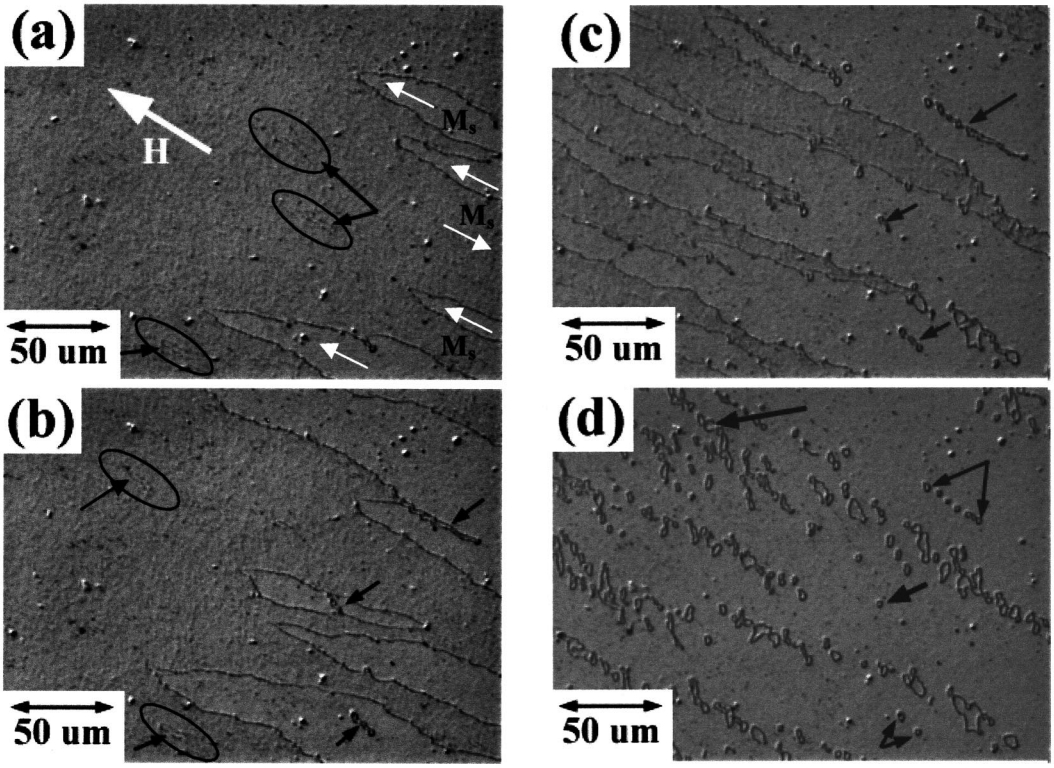

FIG. 5. Domain structure during magnetization reversal in a Co/Cu/Co trilayer along the easy axis. The images were recorded using the ICC technique (see text). The direction of applied field points along the white arrow marked in Fig. 5(a), which coincides with the uniaxial anisotropy axis. Applied field values are (a) $H=2.2$ mT, (b) $H=2.5$ mT, (c) = 2.7 mT, and (d) = 6.1 mT. See text for explanation.

reversal in the ''free'' Co layer to be made without significantly altering the magnetic state of the pinned Co layer. Although the pinned Co layer does not undergo magnetization reversal at low fields at which the ''free'' Co layer switches, it was found that the pinned Co layer does exhibit a progressively higher ripple contrast as the field strength was increased. However, reversal of the ''free'' and pinned Co layers occur by nucleation of reversed domains at critical fields (approximately equal to their respective coercivity values), and domain studies showed that these two processes do not overlap. Also, due to a small positive coupling (+0.36 mT) between the free and pinned Co layers of the spin valve, the reversal sequence in the positive or negative saturation was found to be essentially similar in details. A large magnetic field equal to −150 mT was first applied in the negative direction, which causes the magnetization direction in the two Co layers of the spin valve to align parallel to each other. Following this, the field strength was reduced to zero and increased in the positive direction. In Figs. 7(a)–7(f), the direction of the applied field coincides with the easy axis in the ''free'' Co layer and is marked by a white arrow in Fig. 7(a). Figure 7(a) shows the remanence state of the sample ($H=0$ mT) following saturation in the negative direction. As the field strength was increased further, it was found that there exists a critical field strength ≈ 5.3–5.5 mT at which several reversed domains nucleate, as shown in Fig. 7(b). Subsequent increase in the field strength results in further nucleation of new reversed domains, as well as the growth of existing domains, as shown in Figs. 7(b)–7(e). Note that in contrast to reversal in the Co single film and the Co/Cu/Co trilayer shown in Figs. 4 and 5, respectively, reversal in the ''free'' Co layer of a spin valve is highly local and nonuniform in nature. It also results in the formation of a high density of locked-in domain walls, as shown in Figs. 7(d)–7(f), marked by the arrows. Very large fields, ranging from 10 to 70 mT, were required to annihilate these strongly coupled walls. Therefore, the essential differences in magnetization reversal in the free Co layer of spin valve versus the trilayer are a high density of locked-in domain walls in the former, their greater stability, and a highly local and nonuniform reversal process.

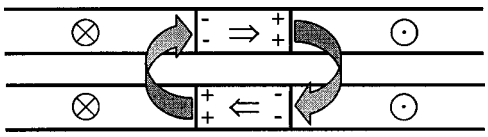

FIG. 6. Schematic of superimposed Néel walls of opposite chilarity in a Co/Cu/Co trilayer. Superimposed Néel walls are energetically favorable entities due to a more complete flux closure associated with them.

IV. DISCUSSION

It was mentioned in the Introduction that various exchange interactions, direct or indirect, might be simultaneously present in a magnetic multilayer, which, in turn, may be positive (parallel) or negative (antiparallel) in nature. The results presented in the previous section allows a distinction to be made as to the nature of the operative coupling mechanisms and origin of enhanced coercivity in the ''free'' Co layer of spin valves. In particular, coupling between the

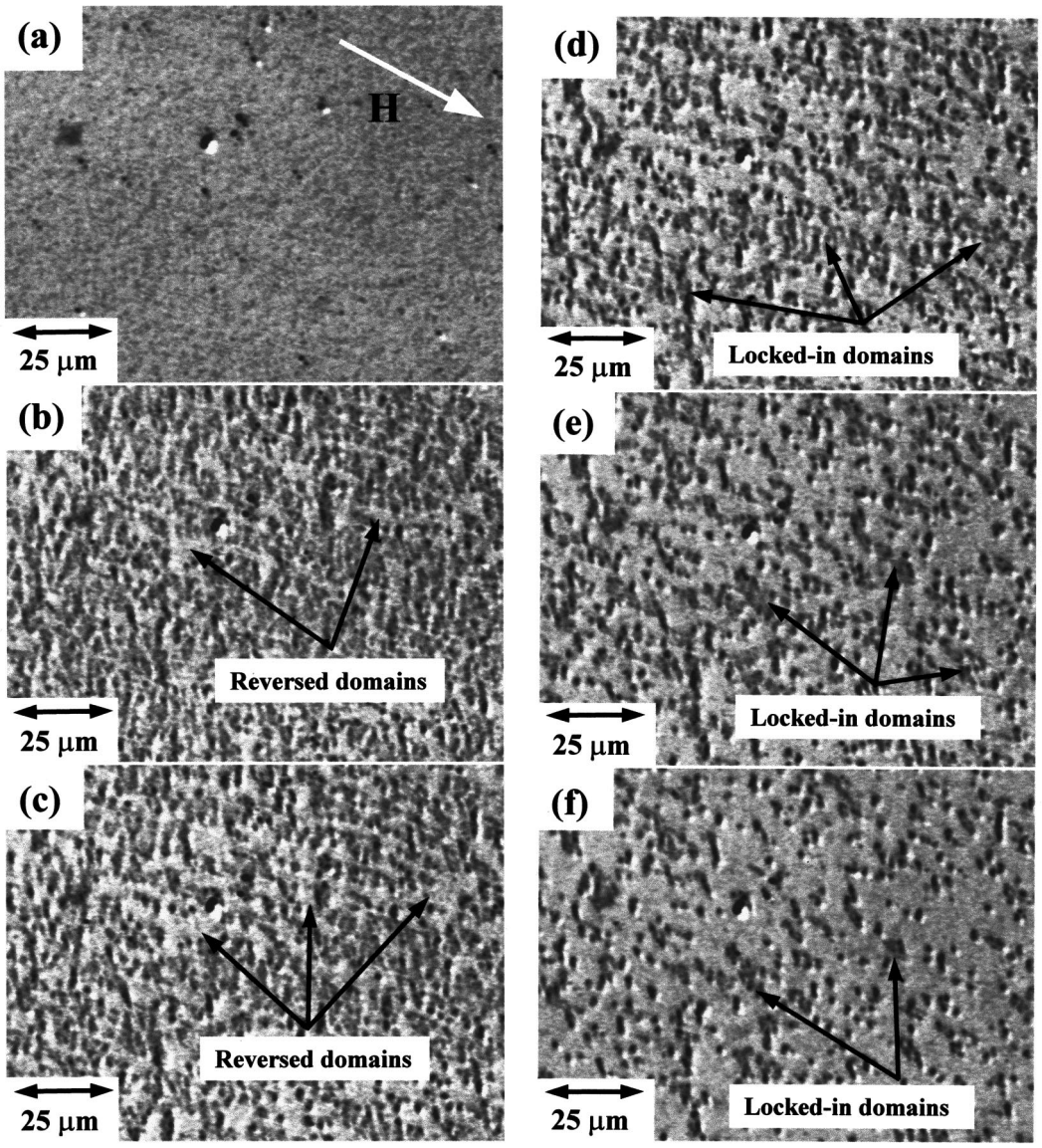

FIG. 7. Domain structure during magnetization reversal in a Co (4.0 nm)/Cu (2.0 nm)/Co (2.5 nm)/NiO (50 nm) bottom spin valve along the easy axis. The images were recorded using the ICC technique (see text). The direction of applied field points along the white arrow marked in Fig. 7(a), which coincides with the uniaxial anisotropy axis. Applied field values are (a) $H=0$ mT, (b) $H=5.5$ mT, (c) = 5.9 mT, (d) = 6.8 mT, (e) = 9.8 mT, and (f) = 11 mT. See text for explanation.

''free'' and pinned Co layers may arise due to (i) the oscillatory exchange coupling (positive or negative),[12] (ii) stray field or demagnetizing coupling (negative),[20,21] (iii) Néel's so-called ''orange-peel'' coupling (positive),[22,23] (iv) magnetostatic coupling due to domain walls in different magnetic layers,[24–30] which is local in nature, and (iv) coupling due to pinholes (positive).[32,33]

Figure 8 shows a typical medium magnification TEM micrograph of a bottom spin valve investigated in the present study. Due to a close proximity of the elements Co ($Z=27$) and Cu ($Z=29$) in the periodic table, images recorded near the optimum Scherzer focus would have little composition contrast, which makes the delineation of the individual Co and Cu layers difficult. However, as shown in Fig. 8, the individual layers as well as the interfaces can be clearly seen by viewing at large defocus, which increases the scattering factor contrast between the two elements and the presence of Fresnel fringes at the Co-Cu interfaces. The contrast between

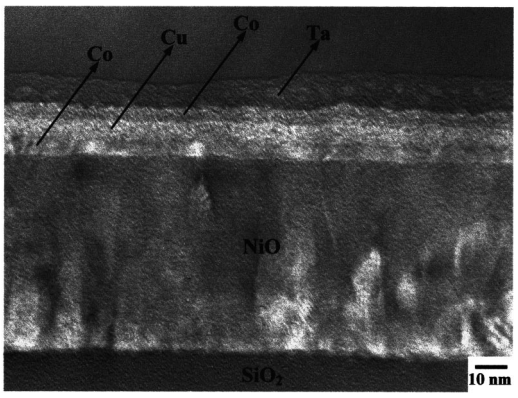

FIG. 8. A TEM micrograph of a NiO-Co-Cu-based bottom spin valve indicating the absence of any pinholes. The top Co layer in this spin valve had a thickness of 3.0 nm instead of 4.0 nm.

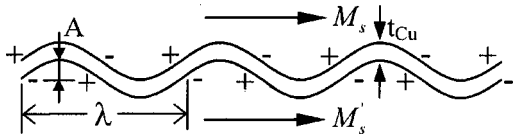

FIG. 9. Schematic of layer geometry giving rise to Néel's ''orange-peel'' coupling in ferromagnetic layers separated by nonmagnetic spacers.

the Co and Cu layers reverse between the overfocused and underfocused conditions. Note that another necessary and important condition for the successful imaging of the Co-Cu interfaces is the extremely precise alignment of the electron beam parallel to the interfaces. A careful examination of Fig. 8, and extensive TEM studies over large areas of the samples revealed that the individual layers of Co and Cu are continuous and without the presence of any interlayer bridging between the Co layers. Therefore, in the absence of pinholes, any contribution to net coupling due to pinholes is discounted for in the present study.

The stray field coupling, on the other hand, is always present in magnetic multilayers. It arises because each ferromagnetic layer is placed in the demagnetizing field of the other, which tends to align the magnetization of adjacent layers antiparallel. Stray field coupling is weak for large lateral dimensions of the film, being inversely proportional to the diameter of the film.[20,21] Since magnetic measurements were made over sufficiently large areas ($\approx$ 1 cm^2 squares), any contribution to net coupling from stray field coupling is also ignored in the present study.

The so-called ''orange-peel'' coupling, enunciated by Néel, is magnetostatic in nature.[22,23] The model considers two ferromagnetic layers with in-plane magnetization, separated by a nonmagnetic spacer. If the surface of ferromagnetic layers has correlated roughness, dipoles are set up at homologous protrusions and bumps at the interfaces, as shown schematically in Fig. 9. Each pair of such homologous protrusion or bump introduces, into the energy of the system an extra energy term, which tends to ferromagnetically align the magnetization in the two magnetic layers. Néel pointed out that under these conditions, the magnetization distribution within the ferromagnetic layers would undergo a transition to a new equilibrium state as a result of this extra magnetostatic energy, which competes with the exchange and uniaxial anisotropy energy terms.[22] Néel further showed that if the correlated roughness is assumed to have in-plane isotropy,[23,50] the coupling energy due to the ''orange-peel'' effect, in the limit of *rigid* in-plane magnetization in the two layers, is given by[23]

$$\varepsilon_{\mathrm{OP}}^{\mathrm{rigid}} = -\frac{\pi^2}{\sqrt{2}\lambda}\mu_0 A^2 M_s M_s' e^{-2\pi t_{\mathrm{Cu}}\sqrt{2}/\lambda}, \tag{1}$$

where M_s and M_s' are values of saturation magnetization of the two ferromagnetic layers, A is the amplitude, and λ is the wavelength of topographically correlated interfaces, which are separated by a nonmagnetic spacer whose thickness is t_{Cu}, as shown in Fig. 9. The negative sign in Eq. (1) shows that the coupling is positive in nature. Following Néel,[23] if the condition of rigid magnetization is relaxed in order to allow the system to undergo a transition to a new equilibrium state of magnetization distribution in the ferromagnetic layers, the coupling energy due to the ''orange-peel'' effect is given by

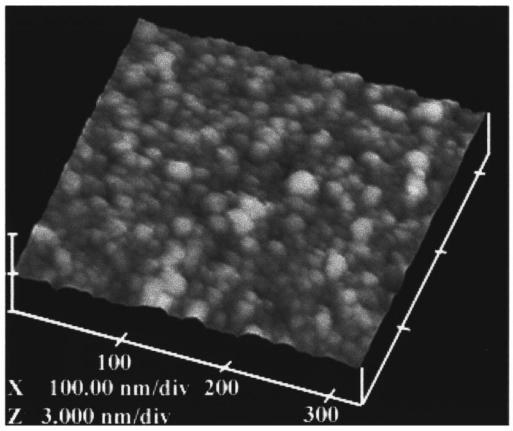

FIG. 10. An *in situ* STM topograph of the ''free'' Co layer of a NiO-Co-Cu-based bottom spin valve.

$$\varepsilon_{\mathrm{OP}} \cong -\frac{2}{5}\frac{\pi^2}{\sqrt{2}\lambda}\mu_0 A^2 M_s M_s' e^{-3t_{\mathrm{Cu}}/\lambda}. \tag{2}$$

Recent nanostructure investigations using HRTEM have shown that the Co and Cu layers in as-deposited spin-valves grow coherently over each other within columnar grains.[34,35] These investigations also showed that a coherent growth mode of the metal layers give rise to topographically correlated ferromagnetic films, a prerequisite if ferromagnetic coupling arises from Néel's ''orange-peel'' effect. Therefore, the relevant scales for λ and A corresponds, respectively, to the grain size and grain roughness of the topographically correlated ferromagnetic layers. In order to calculate the values of λ and A, HRTEM and *in situ* STM studies were performed on spin valves and trilayers, and a typical *in situ* STM topograph of the free Co layer of a bottom spin valve is shown in Fig. 10. These studies show that the average grain size λ in the films is $\approx$20 nm and average roughness A is $\approx$0.3 nm. Using these values, the calculated value of average coupling strength $|\varepsilon_{\mathrm{O-P}}|^{\mathrm{avg}}$ in the film due to the ''orange-peel'' effect, from Eq. (2), is 0.0018 mJ m^{-2}. The net coupling between two ferromagnetic films may also be represented by a coupling energy term E_c. In general, the existence of coupling between two ferromagnetic layers leads to the introduction of a fictitious coupling field h related to E_c by the relation[32]

$$E_c = \mu_0 M_s h t, \tag{3}$$

where t is the thickness of the ferromagnetic layer on which this fictitious field acts. From Fig. 2(b), the shift in the low-field GMR loop away from the center is a measure of h (equal to +0.36 mT). Using Eq. (3), the experimentally determined value of net coupling energy E_c is $\approx$0.002 mJ m^{-2}. Therefore, the measured value of coupling energy E_c correlates well with the calculated value of average coupling energy $|\varepsilon_{\mathrm{OP}}|^{\mathrm{avg}}$ in the film due to the ''orange-peel'' effect. Of course one would expect to find several regions in the film where the grain size and roughness is smaller or larger than this average value, as seen from Figs. 8 and 10. Using Eq.

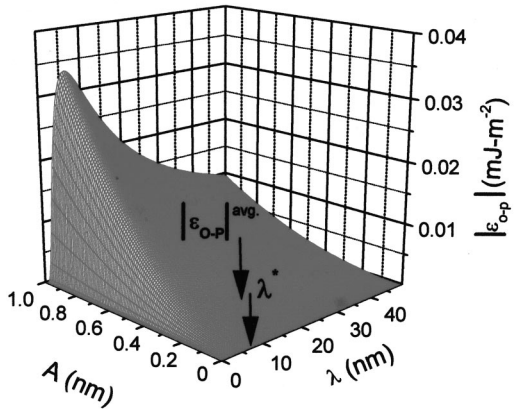

FIG. 11. The variation in absolute value of Néel's ''orange-peel'' coupling $|\varepsilon_{OP}|$ as a function of amplitude A and wavelength λ. Using the values of A and λ obtained from STM and TEM results, the calculated value of $|\varepsilon_{OP}|^{avg}$ in bottom spin valves is indicated by an arrow. Also note the square-amplitude dependence of $|\varepsilon_{OP}|^{max}$ when $3t_{Cu}/\lambda^*=1$; for the given Cu thickness of 2.0 nm, this corresponds to $\lambda^*=6.0$ nm, as marked by the arrow.

(2), Fig. 11 shows the variation in the absolute value of $|\varepsilon_{OP}|$ as a function of wavelength λ and amplitude of roughness A. Equation (2) also shows that the maximum value of coupling $|\varepsilon_{OP}|^{max}$ occurs when $3t_{Cu}/\lambda^*=1$. For the given Cu thickness of 2.0 nm, the maximum coupling strength $|\varepsilon_{OP}|^{max}$ in Co layers occurs at $\lambda^*=6.0$ nm, and is given by

$$\varepsilon_{OP}^{max}=-3.34A^2 10^{16}\ \text{mJ m}^{-2}. \tag{4}$$

This square-amplitude dependence of coupling strength can also be seen from Fig. 11 at $\lambda=\lambda^*=6.0$ nm. An important observation that can be made from Fig. 11 is that the effect of the ''orange-peel'' coupling arising from topographically correlated interfaces may be minimized by depositing films with average grains size relatively larger than λ*. However, as recently noted by Lubitz *et al.*,[41] a small grain size results in the averaging of exchange interactions over several grains, thereby precluding the display of local magnetocrystalline easy axes, which, in turn, would otherwise lead to high switching fields. Therefore, an increase in grain size to reduce ''orange-peel'' coupling should not exceed the characteristic length for this averaging ($\approx\sqrt{A/2\Delta K}$ where A is the exchange constant and ΔK is the anisotropy energy difference per unit volume between adjacent regions), which in the present case is ≈45 nm. Alternatively, since correlated roughness is a prerequisite to ''orange-peel'' coupling, recent studies have shown that a disruption of the coherent growth mode by using surface modifiers, or simply, surfactants, during film growth leads to a disruption of topographically correlated interfaces between adjacent ferromagnetic layers.[34] Using surfactants, coupling due to the ''orange-peel'' effect could almost be eliminated.

Figure 11 also shows that, locally, the strength of ''orange-peel'' coupling may become very large even for small roughness if the grain size becomes comparable to λ*. For instance, the STM topograph in Fig. 10 shows that, indeed, there exist several grains that satisfy this condition. Using Eq. (4), such local regions would then exhibit coupling strength varying between 0.003 and 0.027 mJ m^{-2} for roughness varying between 1 and 3 times the average roughness in the film. Using Eq. (3), this translates into local values of coupling field h ranging from 0.5 to 5.0 mT, respectively. Note that the Co/Cu/Co trilayers were deposited under similar growth conditions as the bottom spin valves, and were found to have similar topographic characteristics. Therefore, these are also the expected variations in coupling in the trilayer due to the ''orange-peel'' effect. Microscopic details of magnetization reversal in the trilayer in Figs. 5 clearly showed that, as the ferromagnetically coupled Co layers were remagnetized, several 360° walls are formed. It was also noted in the previous section that applied fields as high as 10–12 mT are required to annihilate these 360° walls in the trilayer. Therefore, a higher stability of these regions can be explained by taking into account local variation in coupling strength due to the ''orange-peel'' effect. In this regard, also note that a Cu thickness of 2.24 nm corresponds to the second antiferromagnetic peak in the oscillatory exchange coupled Co films as a function of Cu spacer thickness. Below 2.0 nm thickness, the coupling has a very sharp Cu-thickness dependence, with ferromagnetic coupling increasing ≈5 mT for every 0.1 nm decrease in the Cu layer thickness.[34] Therefore, locally the effective Cu thickness in the trilayer also varies due to nonuniform Cu spacer thickness, as seen from Fig. 8, or by elemental intermixing at the Co-Cu interfaces, and these variations could also explain the observed 360° walls in the trilayer. However, *a priori*, it is difficult to unambiguously ascertain as to which of the above two mechanisms dominate (''orange-peel'' or oscillatory exchange), although correlated growth of the metal layers in as-deposited films suggest the former to be the dominant mechanism, with oscillatory coupling also likely to be operative.

Since the spin valves were deposited under similar growth conditions as the trilayer and have similar topographic characteristics, the ''free'' Co layer could be expected to exhibit switching characteristics similar to those shown in Figs. 5 for the trilayer, after taking into account the above described contributions to net coupling from orange-peel and oscillatory exchange effects. However, Figs. 7 clearly shows that the density of locked-in domains in the ''free'' Co layer of spin valves is considerably higher than that in the trilayer. Furthermore, the stability of locked-in regions in the ''free'' Co layer is also higher (up to 70 mT) than that in the trilayer (up to 12 mT). Also, whereas a coercivity enhancement is observed in the ''free'' Co layer of the spin valves ($H_c^{\text{Free-Co}}=6.7$ mT), coercivity of the Co layers in the trilayer ($H_c^{\text{Co/Cu/Co}}=3.0$ mT) remains largely unchanged with respect to the Co single film ($H_c^{\text{Co}}=2.7$ mT). These differences may be explained by considering the localized magnetostatic interaction between stray fields associated with domain walls or magnetization ripples in magnetic layers separated by nonmagnetic spacers. Fuller and Sullivan showed that *if the coercivity of individual layers differ significantly* (as is the case for spin valves and in contrast to the Co/Cu/Co trilayer), the stray fields emanating from high coercive force domain walls (and also any other source of stray fields such as magnetization ripples) in the magnetically hard layer can magnetostatically lock-in the stray fields associated with domain walls (and magnetization ripples) in the soft layer.[24] Fuller and Sullivan further showed, both experimentally and theo-

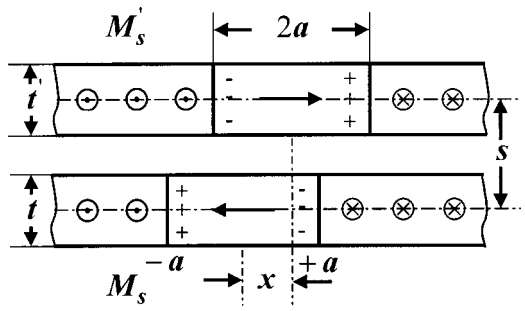

FIG. 12. Definition of parameters describing magnetostatic coupling between domain walls in ferromagnetic layers separated by nonmagnetic spacers.

retically, that domain walls in the soft layer require large escape field values in order to overcome magnetostatic coupling with the hard layer.[24,25] They showed that the theoretical value of the escape field H^{esc} for a domain wall in the soft layer, in excess of its coercive force, is given by the equation[24]

$$-\frac{aH^{esc}}{8M_s t}=\frac{u[u^2-(3\sigma^2+4)]}{[\sigma^2+(u+2)^2][\sigma^2+(u-2)^2][\sigma^2+u^2]}, \quad (5)$$

where, $u=x/a$, $\sigma=s/a$, t and t' are the thickness of the hard and the soft magnetic layers, respectively, and M_s and M_s' are the respective saturation magnetization of the hard and the soft layers (see Fig. 12). Following Fuller and Sullivan,[24,25] the force function $(aH^{esc})/(8M_s t)$ given by Eq. (5) is plotted for positive values of u in Fig. 13, for σ equal to 0.5, 0.3, and 0.2 (see Ref. 51). For these value of σ, Fig. 13 shows that the force function reaches a maximum value of 0.275, 0.425, and 0.625, respectively. From this, the theoretical values of H^{esc} lie between ≈77 and 44 mT, respectively, and for applied field $H>H^{esc}$ a domain wall in the soft layer will escape the local magnetostatic interaction field in the hard layer. (The value of 44 mT obviously corresponds to the coercivity of the pinned Co layer. From the previous section, the experimental values of H^{esc} in the ''free'' Co layer lie between 10 and 70 mT. As discussed above, the lower values in this range can be interpreted on the basis of coupling due to the ''orange-peel'' and/or oscillatory exchange effects. From Eq. (5), the upper limits of this range are expected on the basis of magnetostatic interaction between domain walls. Furthermore, a variation in the observed H^{esc} can be qualitatively explained by noting that the pole density associated with magnetization ripples (that can be approximated as quasiwalls) would be lower than that for a domain wall. Modified, accordingly, Eq. (5) would then predict lower values of H^{esc}. Indeed, in-depth investigations of magnetization reversal in Co/NiO bilayers being reported elsewhere show that in the range of applied fields necessary to switch the ''free'' Co layer, the NiO-pinned Co layer exhibits a progressively enhanced ripple contrast, in addition to the presence of some immobile domain walls.[42] Based on these results, the magnetostatic coupling due to stray fields associated with ripples (akin to quasidomain walls) in the pinned-Co layer is deemed to be the dominant mode of interaction in the present samples. The development of progressively enhanced ripple contrast as the applied field strength is increased is also further supported by the recent magnetic-force microscopy results by McMichael *et al.*[52] Another mechanism leading to lower H^{esc} for a domain wall in the soft layer is the motion of a domain wall in the hard layer itself arising from local variations in its wall coercive force. In the limit where the wall coercivity in the two Co layers become the same, H^{esc} approaches the coercivity of the layers, as was the case for the trilayer. A large difference in coercivity in the two magnetic layers is a prerequisite for high H^{esc}.

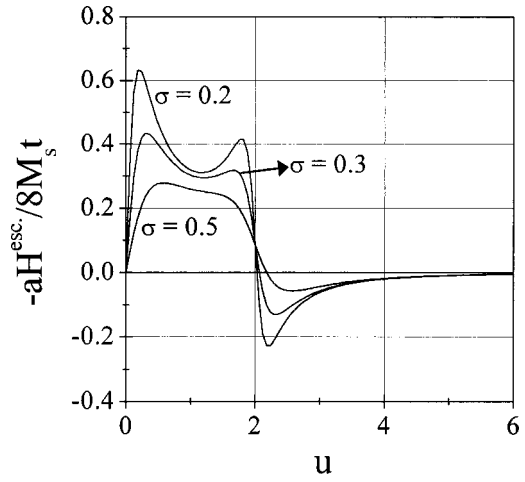

FIG. 13. Variation of $(aH^{esc})/(8M_s t)$ as a function of u for different parametric values of σ.

V. CONCLUSIONS

A systematic analysis and quantitative estimation of the magnitude of coupling strength due to different mechanisms, their manifestation during switching, and the origin of often observed coercivity enhancement in the ''free'' Co layer of bottom spin valves is made in the present study. As-deposited bottom spin valves exhibit a large GMR of ≈16.5%, and a small net ferromagnetic coupling (+0.36 mT) between the ''free'' Co layer and the NiO-pinned Co layer. The HRTEM and *in situ* STM studies on spin valves and trilayers show that the average grain size in these films is ≈20 nm and average roughness ≈0.3 nm. In addition, TEM results discount the possibility of any interlayer bridging between the Co layers across the Cu spacer layer. Using the measured values of roughness amplitude and wavelength, the observed ferromagnetic coupling in spin valves could largely be accounted for by Neel's so-called ''orange-peel'' coupling arising due to correlated interfaces. Results also show that the ''free'' Co layer exhibits an enhanced coercivity ($H_c^{\text{Free-Co}}=6.7$ mT) with respect to Co single films of comparable thickness ($H_c^{\text{Co}}=2.7$ mT).

The nature of magnetization reversal and measurement of M-H loops in these films show that the observed coercivity enhancement in the ''free'' Co layer results from magnetostatic coupling between domain walls in the ''free'' Co layer and high coercivity NiO-pinned Co layer ($H_c^{\text{Pinned-Co}}\approx 45$ mT); without NiO, the coercivity of Co layers in the corresponding Co/Cu/Co trilayer remains largely unchanged ($H_c^{\text{Co/Cu/Co}}=3.0$ mT) with respect to Co single films.

That magnetostatically coupled domain walls are the origin of coercivity enhancement in the ''free'' Co layer of spin

valves was confirmed by direct observation of magnetization reversal, which revealed that domain walls in the ''free'' Co layer are magnetostatically locked-in with stray fields due to domain walls or magnetization ripples in the high coercivity NiO-pinned Co layer of the spin valves.

The observed escape fields, in excess of the intrinsic coercivity of the Co single film, required to overcome magnetostatic coupling between domain walls are in agreement with theoretically calculated values of escape fields.

ACKNOWLEDGMENTS

This work was supported by the National Science Foundation, Grant No. DMR-97-31733, and this support is gratefully acknowledged.

*Author to whom correspondence should be addressed. Electronic address: hchopra@eng.buffalo.edu

[1] M. B. Saloman, S. Sinha, J. J. Rhyne, J. E. Cunningham, R. W. Erwin, and C. P. Flynn, Phys. Rev. Lett. **56**, 259 (1986).
[2] C. F. Majkrzak, J. M. Cable, J. Kwo, M. Hong, D. B. Mcwhan, Y. Yafet, and C. Vettier, Phys. Rev. Lett. **56**, 2700 (1986).
[3] J. R. Dutcher, B. Heinrich, J. F. Cochran, D. A. Steigerwald, and W. F. Egelhoff, Jr., J. Appl. Phys. **63**, 3464 (1988).
[4] P. Grünberg, R. Schreiber, Y. Pang, M. B. Brodsky, and H. Sowers, Phys. Rev. Lett. **57**, 2442 (1986).
[5] F. Saurenbach, U. Walz, L. Hinchey, P. Grünberg, and W. Zinn, J. Appl. Phys. **63**, 3473 (1988).
[6] H. Ohno, Science **281**, 951 (1998).
[7] G. Prinz, Science **282**, 1660 (1998).
[8] E. Velu, C. Dupas, D. Renard, J. P. Renard, and J. Seiden, Phys. Rev. B **37**, 668 (1988).
[9] E. D. Dahlberg, K. Riggs, and G. A. Prinz, J. Appl. Phys. **63**, 4270 (1988).
[10] M. N. Baibich, J. M. Broto, A. Fert, F. Nguyen Van Dau, F. Petroff, P. Etienne, G. Creuzet, A. Friederich, and J. Chazelas, Phys. Rev. Lett. **61**, 2472 (1988).
[11] G. Binash, P. Grünberg, F. Saurenbach, and W. Zinn, Phys. Rev. B **39**, 4828 (1989).
[12] S. S. P. Parkin, N. More, and K. P. Roche, Phys. Rev. Lett. **64**, 2304 (1990).
[13] L. M. Falicov, Phys. Today **45** (10), 46 (1992).
[14] H. Kano, K. Kagawa, A. Suzuki, A. Okabe, K. Hayashi, and K. Aso, Appl. Phys. Lett. **63**, 2839 (1993).
[15] T. C. Anthony, J. A. Brug, and S. Zhang, IEEE Trans. Magn. **30**, 3819 (1994).
[16] V. S. Speriosu, B. Dieny, P. Humbert, B. A. Gurney, and H. Lefakis, Phys. Rev. B **44**, 5358 (1991).
[17] B. Dieny, V. S. Speriosu, S. S. P. Parkin, B. A. Gurney, D. R. Wilhoit, and D. Mauri, Phys. Rev. B **43**, 1297 (1991).
[18] C. Meny, J. P. Jay, P. Panissod, P. Humbert, V. S. Speriousu, H. Lefakis, J. P. Nozieres, and B. A. Gurney, in *Magnetic Ultrathin Films: Multilayers and Surfaces/Interfaces and Characterization*, edited by B. T. Jonker *et al.*, MRS Symposia Proceedings No. 313 (Materials Research Society, Warrendale, PA, 1990), p. 289.
[19] D. Dieny, J. Magn. Magn. Mater. **136**, 335 (1994).
[20] L. J. Oakland and T. D. Rossing, J. Appl. Phys. **30**, 54S (1959).
[21] J. C. Suits and E. W. Pugh, J. Appl. Phys. **33**, 1057 (1962).
[22] L. Néel, C. R. Hebd. Seances Acad. Sci. **255**, 1545 (1962).
[23] L. Néel, C. R. Hebd. Seances Acad. Sci. **255**, 1676 (1962).
[24] H. W. Fuller and D. L. Sullivan, J. Appl. Phys. **33**, 1063 (1962).
[25] H. W. Fuller and L. R. Lakin, J. Appl. Phys. **34**, 1069 (1963).
[26] S. Middelhoek, J. Appl. Phys. **37**, 1276 (1966).
[27] J. C. Slonczewski, Phys. Rev. Lett. **67**, 3172 (1991).
[28] H. Clow, Nature (London) **4833**, 1035 (1962).
[29] F. Feldtkeller, J. Appl. Phys. **39**, 1181 (1968).
[30] J. C. Slonczewski and S. Middelhoek, Appl. Phys. Lett. **6**, 139 (1965).
[31] J. Unguris, R. J. Celotta, and D. T. Pierce, Phys. Rev. Lett. **67**, 140 (1991).
[32] J. C. Bruyère, O. Massanet, R. Montmory, and L. Néel, IEEE Trans. Magn. **1**, 10 (1965).
[33] J. C. Bruyère, O. Massanet, R. Montmory, and L. Néel, C. R. Acad. Sci., Ser. A **258**, 841 (1964).
[34] H. D. Chopra, B. J. Hockey, P. J. Chen, W. F. Egelhoff, Jr., M. Wuttig, and S. Z. Hua, Phys. Rev. B **55**, 8390 (1997).
[35] H. D. Chopra, B. J. Hockey, P. J. Chen, R. D. McMichael, and W. F. Egelhoff, Jr., J. Appl. Phys. **81**, 4017 (1997).
[36] D. A. Steigerwald, I. Jacob, and W. F. Egelhoff, Jr., Surf. Sci. **202**, 472 (1988).
[37] W. F. Egelhoff, Jr. and D. A. Steigerwald, J. Vac. Sci. Technol. A **7**, 2167 (1989).
[38] W. F. Egelhoff, Jr., P. J. Chen, R. D. K. Misra, T. Ha, Y. Kadmon, C. J. Powell, M. D. Stiles, R. D. McMichael, C.-L. Lin, J. M. Sivertsen, and J. H. Judy, J. Appl. Phys. **79**, 282 (1996).
[39] W. F. Egelhoff, Jr., P. J. Chen, C. J. Powell, M. D. Stiles, R. D. McMichael, J. H. Judy, K. Takano, and A. E. Berkowitz, J. Appl. Phys. **82**, 6142 (1997).
[40] W. F. Egelhoff, Jr., P. J. Chen, C. J. Powell, M. D. Stiles, and R. D. McMichael, J. Appl. Phys. **79**, 2491 (1996).
[41] P. Lubitz, Shu-Fan Cheng, K. Bussman, G. A. Prinz, J. J. Krebs, J. M. Daughton, and D. Wang, J. Appl. Phys. **85**, 5027 (1999).
[42] H. D. Chopra, D. X. Yang, P. J. Chen, H. J. Brown, L. J. Swartzendruber, and W. F. Egelhoff, Jr., Phys Rev. B (to be published); D. X. Yang, H. D. Chopra, P. J. Chen, H. J. Brown, L. J. Swartzendruber, and W. F. Egelhoff, Jr., J. Appl. Phys. (to be published 15 April 2000).
[43] U. Hartmann and H. H. Mende, J. Phys. D **18**, 2285 (1985).
[44] H. D. Chopra, S. Z. Hua, D. S. Lashmore, M. Wuttig, R. D. Shull, W. F. Egelhoff, Jr., and L. J. Swartzendruber, Microsc. and Analysis **28**, 15 (1998); European Microsc. Anal. **28**, 27 (1998).
[45] G. Nomarski and A. R. Weil, Rev. Met. **52**, 121 (1955).
[46] Note that in the reflection mode, the Nomarski interferometer develops contrast due to the angle difference rather than the step height difference between the two rays.
[47] The coercivity of Co single films was measured for film thickness ranging from 2.5 to 10 nm and H_c^{Co} was found to lie between $\approx$2.7 and 3.0 mT.
[48] L. J. Heyderman, H. Niedoba, H. O. Gupta, and I. B. Puchalska, J. Magn. Magn. Mater. **96**, 125 (1991).
[49] L. J. Heyderman, J. N. Chapman, and S. S. P. Parkin, J. Magn. Magn. Mater. **138**, 344 (1994).
[50] In Ref. 23, Néel has shown that if the roughness is correlated only along one direction as opposed to all the directions in the plane of the film, then $\varepsilon_{\mathrm{OP}}^{1-d} \cong 4\varepsilon_{\mathrm{OP}}^{\mathrm{isotropic}}$. Therefore, the existence of any topographic texture in the films may lead to substantially higher values of ''orange-peel'' coupling in comparison to films,

which have isotropic topographs. Also see Ref. 34 for experimental validation for the same.

[51] In comparison to domain-wall width $w^{\text{single film}} = 2a \cong \pi\sqrt{A/2K}$ in magnetic single films, calculation and experimental determination of wall width in magnetic multilayers (Refs. 26–30) show that the wall width increases and wall energy decreases in magnetic multilayers. This is due to a more complete closure of stray fields associated with domain walls in magnetic multilayers due to interlayer interactions, which is not feasible in magnetic single films. Therefore, variation of $(aH^{\text{esc}})/(8M_s t)$ as a function of u is plotted for σ varying from 0.5 (corresponding to $w^{\text{single film}} \approx 20$ nm) to 0.2 (corresponding to $w \approx 4w^{\text{single film}} = 80$ nm in magnetic multilayers following Refs. 26–30).

[52] R. D. McMichael, P. J. Chen, and W. F. Egelhoff, Jr. (unpublished).